

# Localization of the source of quasiperiodic VLF emissions in the magnetosphere by using simultaneous ground and space observations: a case study

Andrei G. Demekhov<sup>1</sup>, Elena E Titova<sup>2</sup>, Jyrki Maninnen<sup>3</sup>, Andris A. Lubchich<sup>2</sup>, Alexey V. Larchenko<sup>2</sup>, Dmitry Pasmanik<sup>4</sup>, Ondrej Santolík<sup>5</sup>, Tauno Turunen<sup>6</sup>, and Alexander Nikitenko<sup>2</sup>

<sup>1</sup>Institute of Applied Physics, Russian Academy of Sciences

<sup>2</sup>Polar Geophysical Institute

<sup>3</sup>Sodankylä Geophysical Observatory

<sup>4</sup>Institute of Applied Physics Russian Academy of Science

<sup>5</sup>Department of Space Physics, Institute of Atmospheric Physics, The Czech Academy of Sciences, Prague, Czech Republic

<sup>6</sup>Sodankylä Geophysical Observatory

November 24, 2022

## Abstract

We study quasi-periodic VLF emissions observed simultaneously by Van Allen Probes spacecraft and Kannuslehto and Lovozero ground-based stations on 25 December 2015. Both Van Allen Probes A and B detected quasi-periodic emissions, probably originated from a common source, and observed on the ground. In order to locate possible regions of wave generation, we analyze wave normal angles with respect to the geomagnetic field, Poynting flux direction, and cyclotron instability growth rate calculated by using the measured phase space density of energetic electrons. We demonstrate that even parallel wave propagation and proper (downward) Poynting flux direction are not sufficient for claiming observations to be in the source region. Agreement between the growth rate and emission bands was obtained for a restricted part of Van Allen Probe A trajectory corresponding to localized enhancement of plasma density with scale of 700 km. We employ spacecraft density data to build a model plasma profile and to calculate ray trajectories from the point of wave detection in space to the ionosphere, and examine the possibility of their exit to the ground. For the considered event, the wave could exit to the ground in the geomagnetic flux tube with enhanced plasma density, that ensured ducted propagation. The region of wave exit was confirmed by the analysis of wave propagation direction at the ground detection point.

1                   **Localization of the source of quasiperiodic VLF**  
2                   **emissions in the magnetosphere by using simultaneous**  
3                   **ground and space observations: a case study**

4                   **A. G Demekhov<sup>1,2</sup>, E. E. Titova<sup>1,3</sup>, J. Manninen<sup>4</sup>, D. L. Pasmanik<sup>2</sup>, A. A.**  
5                   **Lubchich<sup>1</sup>, O. Santolík<sup>5,6</sup>, A. V. Larchenko<sup>1</sup>, A. S. Nikitenko<sup>1</sup>, and T.**  
6                   **Turunen<sup>4</sup>**

7                                   <sup>1</sup>Polar Geophysical Institute, Apatity, Russia

8                                   <sup>2</sup>Institute of Applied Physics, RAS, Nizhny Novgorod, Russia

9                                   <sup>3</sup>Space Research Institute, RAS, Moscow, Russia

10                                  <sup>4</sup>Sodankylä Geophysical Observatory, Sodankylä, Finland

11                                  <sup>5</sup>Department of Space Physics, Inst. Atmospher. Phys., Czech Acad. Sci., Prague, Czechia

12                                  <sup>6</sup>Faculty of Mathematics and Physics, Charles University in Prague, Czechia

13                   **Key Points:**

- 14                   • Complex analysis of generation region of quasi-periodic VLF emissions observed  
15                   simultaneously by two Van Allen Probes and on the ground
- 16                   • Wave growth rate frequency band matched the observed emission band in a lo-  
17                   calized region along Van Allen Probe A trajectory
- 18                   • Ray tracing demonstrated the importance of a density duct for wave exit to the  
19                   ground

---

Corresponding author: Andrei Demekhov, [andrei@ipfran.ru](mailto:andrei@ipfran.ru)

**Abstract**

We study quasi-periodic VLF emissions observed simultaneously by Van Allen Probes spacecraft and Kannuslehto and Lovozero ground-based stations on 25 December 2015. Both Van Allen Probes A and B detected quasi-periodic emissions, probably originated from a common source, and observed on the ground. In order to locate possible regions of wave generation, we analyze wave normal angles with respect to the geomagnetic field, Poynting flux direction, and cyclotron instability growth rate calculated by using the measured phase space density of energetic electrons. We demonstrate that even parallel wave propagation and proper (downward) Poynting flux direction are not sufficient for claiming observations to be in the source region. Agreement between the growth rate and emission bands was obtained for a restricted part of Van Allen Probe A trajectory corresponding to localized enhancement of plasma density with scale of 700 km. We employ spacecraft density data to build a model plasma profile and to calculate ray trajectories from the point of wave detection in space to the ionosphere, and examine the possibility of their exit to the ground. For the considered event, the wave could exit to the ground in the geomagnetic flux tube with enhanced plasma density, that ensured ducted propagation. The region of wave exit was confirmed by the analysis of wave propagation direction at the ground detection point.

**1 Introduction**

There are many different types of natural electromagnetic VLF emissions, such as hiss, chorus, and quasiperiodic emissions observed both on the ground and by spacecraft for more than 50 years. A rich collection of early observations was presented by Helliwell (1965). It is generally accepted that these types of VLF emissions are generated due to electron cyclotron interaction with energetic electrons (Trakhtengerts, 1963; Kennel & Petschek, 1966).

Recently, characteristics of the sources of different types of VLF emission generated during the development of the cyclotron instability in the magnetosphere have been actively discussed. For this purpose, multispacecraft measurements of VLF waves are often used. For example, Santolík and Gurnett (2003) analyzed individual elements of VLF chorus on four Cluster satellites at  $L = 4.4$ , determined the typical coherence scale of the chorus amplitude of about 100 km across the geomagnetic field which is of the order of the wavelength. Using coordinated observations of Van Allen Probe and THEMIS,

52 Li et al. (2015) confirmed the idea that chorus waves generated at high  $L$  shell ( $\sim 10$ )  
53 can be a source of plasmaspheric hiss (Chum & Santolík, 2003; Santolík et al., 2006; Bort-  
54 nik et al., 2009).

55 Simultaneous ground and satellite observations of the same VLF emissions were  
56 also used for localizing their source. However, such observations are still quite rare. Most  
57 of them deal with quasiperiodic (QP) emissions that are characterized by periodic or quasiperi-  
58 odic modulation of wave intensity with periods from several seconds to minutes. Their  
59 main properties are described in a review by Sazhin and Hayakawa (1994). Similarity  
60 of the frequency-time spectra of quasiperiodic (QP) emissions detected simultaneously  
61 by the low-orbiting DEMETER satellite ( $h \approx 700$  km) and on the ground was reported  
62 by Němec et al. (2016). During those events, the spacecraft crossed a wide range of in-  
63 variant latitudes, which, to our mind, might indicate the nonducted propagation of the  
64 VLF signals. However, the variation of the intensity with the spacecraft latitude indi-  
65 cates, according to Němec et al. (2016) that the sources of QP emissions detected on the  
66 ground were near the plasmopause and the waves propagated along it in the waveguide  
67 regime described by Inan and Bell (1977) and Semenova and Trakhtengerts (1980). Němec  
68 et al. (2018) showed that the majority of QP observations onboard Van Allen Probes (Ra-  
69 diation Belt Storm Probes, hereafter RBSP) took place in the plasmasphere.

70 Recently, QP emissions detected both on the ground and by Van Allen Probes space-  
71 craft in the equatorial region were compared (Titova et al., 2015; Martinez-Calderon et  
72 al., 2016). One-to-one correspondence between the quasiperiodic elements detected on  
73 the ground and by Van Allen Probe-A (RBSP-A) was found in a wide range of  $L$  shells  
74 from 3.0 to 4.3 (Titova et al., 2015), which was explained by nonducted propagation of  
75 QP emissions. By comparing the wave properties and the evolution of electron distri-  
76 bution function during the event, Titova et al. (2015) identified the possible location of  
77 QP emissions source at about  $L = 4$ , and its radial extent was  $\Delta L \approx 0.3$ , i.e., much  
78 smaller than the region of wave observation. This conclusion was further confirmed by  
79 calculations of the wave growth rate on the basis of the measured energetic-electron dis-  
80 tribution (Lyubchich et al., 2017). Martinez-Calderon et al. (2019) analyzed ERG ob-  
81 servations, and their results also indicate that the QP emissions can be detected outside  
82 of the generation flux tube.

83 QP emissions detected at subauroral latitudes on the ground and by RBSP-A in  
 84 the equatorial region were compared by Martinez-Calderon et al. (2016). The similar-  
 85 ity of dynamic spectra of QP elements was demonstrated and the time delay of conju-  
 86 gate QP elements was determined for one element. Based on spacecraft measurements  
 87 of the plasma density, the authors calculated the trajectories of nonducted VLF waves  
 88 and thus explained the observed delay between the QP elements detected by the satel-  
 89 lite and the ground-based station. Therefore Martinez-Calderon et al. (2016) concluded  
 90 that the quasi-periodic emissions detected at a subauroral ground station propagated  
 91 in the nonducted mode in the magnetosphere. Němec et al. (2013) also demonstrated  
 92 that QP emissions observed by the Cluster spacecraft often propagate from the equa-  
 93 tor in a nonducted mode, i.e., obliquely with respect to the magnetic field lines. It is clear  
 94 that nonducted propagation significantly complicates the localization of the source re-  
 95 gion of QP emissions. On the other hand, Manninen et al. (2014) analyzed the periodic  
 96 fine structure of QP elements observed by the ground based subauroral station Kannusle-  
 97 hto (KAN) in Northern Finland, and revealed its correspondence to the time scales of  
 98 guided field-aligned propagation of whistler-mode waves. Based on this fact they con-  
 99 cluded that the QP emissions observed at KAN propagated in the ducted regime. Demekhov  
 100 et al. (2017) and Titova et al. (2017) analyzed simultaneous observations of VLF emis-  
 101 sions at KAN and by RBSP for the event of December 25, 2015, when chorus, QP emis-  
 102 sions, and unstructured hiss were recorded. Those authors have shown that the exit of  
 103 VLF signals, including QP emissions, to the ground was possible due to the wave guid-  
 104 ing in the observed ducts with enhanced density.

105 Němec et al. (2018) have shown that the majority of QP emissions observed by Van  
 106 Allen Probes in the equatorial region had low wave normal angles ( $< 20^\circ$ ). However,  
 107 that conclusion was made by using only waves with sufficiently high planarity ( $p > 0.5$ ),  
 108 which constitute about 1/4 of all events. Overall, the question how the QP emissions prop-  
 109 agate in the magnetosphere and exit to ground has not yet been answered.

110 In this paper, we try to localize the possible generation region of the QP emissions  
 111 and study the mechanism of their exit to the ground for a specific QP event with a pe-  
 112 riod of about 20-30 s detected simultaneously at KAN, Lovozero station (LOZ), and by  
 113 Van Allen Probes on 25 December 2015. The used data are described in Section 2, and  
 114 the observations are presented in Section 3. As the preliminary criteria of the possible  
 115 source location, we use quasi-parallel propagation of the whistler mode waves detected

116 by Van Allen Probes and their Poynting flux direction from the geomagnetic equator.  
 117 However, a more careful analysis turns out to be necessary. In Section 4.1 we calculate  
 118 the growth rate of whistler mode waves by using the spacecraft measurements of ener-  
 119 getic particles and compare it with the spectrum and intensity of the observed VLF waves.  
 120 Agreement between the growth rate and VLF wave spectra together with off-equatorial  
 121 Poynting flux direction and quasi-parallel wave propagation is considered as a more re-  
 122 liable indicator of possible source location. In Section 4.2, we consider the VLF wave prop-  
 123 agation by using ray tracing calculations and analyze conditions for the wave exit to the  
 124 ground. Section 5 presents our conclusions.

## 125 **2 Data**

126 The twin Van Allen Probes spacecraft were launched on 30 August 2012 into near-  
 127 equatorial elliptical orbits with  $\approx 700$  km perigee and  $\approx 5.8R_E$  apogee. Both RBSP-  
 128 A and RBSP-B spacecraft have the same orbit, but RBSP-A has a delay of about 1 h.  
 129 In this paper, we use VLF wave and plasma density measurements from both spacecraft.

130 The wave measurements were made by the Electric and Magnetic Field Instrument  
 131 Suite and Integrated Science (EMFISIS) that provides data on DC magnetic fields and  
 132 three components of electric and magnetic fields (Kletzing et al., 2013). We used the data  
 133 from the survey mode available from the EMFISIS wave instrument. In this mode, the  
 134 EMFISIS/WAVES instrument measures the wave power spectral densities, relative phases,  
 135 and coherencies of electric and magnetic field components from 2 Hz up to 12 kHz in 0.5-  
 136 s intervals every 6 s. This data set allowed us to obtain power spectral density and per-  
 137 form multicomponent wave analysis of ELF/VLF events (Santolík et al., 2014), as a re-  
 138 sult of which one can obtain the polarization of waves (Santolík & Gurnett, 2002), the  
 139 wave-normal angles with the singular-value decomposition (SVD) method of (Santolík  
 140 et al., 2003), and the Poynting vector using the spectral matrix method of (Santolík et  
 141 al., 2010). The in situ cold plasma density was taken from the data on floating space-  
 142 craft potential provided by the Electric Fields and Waves (EFW) instrument (Wygant  
 143 et al., 2013) for RBSP-B. We verified that they agreed well with EMFISIS data based  
 144 on upper hybrid resonance emission (Kurth et al., 2015).

145 Fluxes of particles with energies of a few eV to tens of keV are recorded by HOPE  
 146 (Helium, Oxygen, Proton, and Electron Mass Spectrometer) (Funsten et al., 2013). The

147 fluxes of electrons and protons (as well as helium and oxygen ions) are measured at 11  
 148 pitch-angles from  $4.5^\circ$  to  $175.5^\circ$  and in 72 energy channels with a time resolution of  $\sim$   
 149 20 s. The energy range is from 15 eV to 50 keV for electrons. The fluxes of particles  
 150 with energies of tens of keV to a few MeV with a time resolution of  $\sim 10$  s are measured  
 151 by the MagEIS (The Magnetic Electron Ion Spectrometer) (Blake et al., 2013). These  
 152 fluxes are measured in 23 energy channels from 36 keV to  $\sim 4$  MeV at 11 pitch-angles  
 153 in the range from  $8^\circ$  to  $172^\circ$ .

154 Ground-based observations of VLF signals were carried out in Northern Finland  
 155 at KAN ( $67.74^\circ\text{N}$ ,  $26.27^\circ\text{E}$ ;  $L = 5.45$ ) and LOZ ( $67.98^\circ\text{N}$ ,  $35.08^\circ\text{E}$ ;  $L = 4.96$ ). VLF  
 156 emissions at KAN were recorded in the frequency band from 0.2 to 39 kHz by using two  
 157 mutually orthogonal magnetic loop antennas oriented in the geographical north-south  
 158 and east-west directions. This allows one to calculate polarization characteristics of the  
 159 signal and, in particular, to determine the azimuthal orientation of the polarization el-  
 160 lipse. The small axis direction gives approximate azimuth of VLF wave propagation with  
 161 an ambiguity of  $180^\circ$ . Hereafter we term it the angle of arrival. The loops size is  $10 \times$   
 162 10 m with an effective area of 1000 m<sup>2</sup>. The receiver sensitivity is about 0.1 fT, (i.e.  $\approx$   
 163  $10^{-14}$  nT<sup>2</sup> Hz<sup>-1</sup>). More detailed description of the hardware is given in Manninen (2005).  
 164 The wide dynamic range of the receiver (up to 120 dB) allows us to detect both very weak  
 165 and intense signals. The receiver at LOZ uses a similar magnetic antenna setup with  $15 \times$   
 166 16 m loops having 14 turns. In addition, there is a vertical electric field sensor that can  
 167 be used to remove the  $180^\circ$  ambiguity of propagation direction. Details of the LOZ hard-  
 168 ware can be found in Fedorenko et al. (2014).

### 169 **3 Observations**

170 The event occurred on 25 December 2015 from 11:00 to 13:00 UT. During this time  
 171 interval, the QP VLF emissions were observed at KAN and LOZ in frequency band  
 172  $f = 3\text{--}6$  kHz with periods of 20–30 s. Geomagnetic activity was fairly low with the Dst  
 173 index  $-4$  nT,  $Kp = 2$  and  $AE \approx 100$  nT. Figure 1 shows, in geographic coordinates,  
 174 the relative position of KAN and LOZ and the field-aligned projections of the RBSP-  
 175 A and RBSP-B satellites to the ground in the northern hemisphere. The parts of space-  
 176 craft trajectories at which QP emissions had one-to-one correspondence to those detected  
 177 at KAN are indicated by bold line segments. During the event both satellites were at  
 178 lower geographic latitudes relative to KAN and moved inward. RBSP-B moved from  $L =$

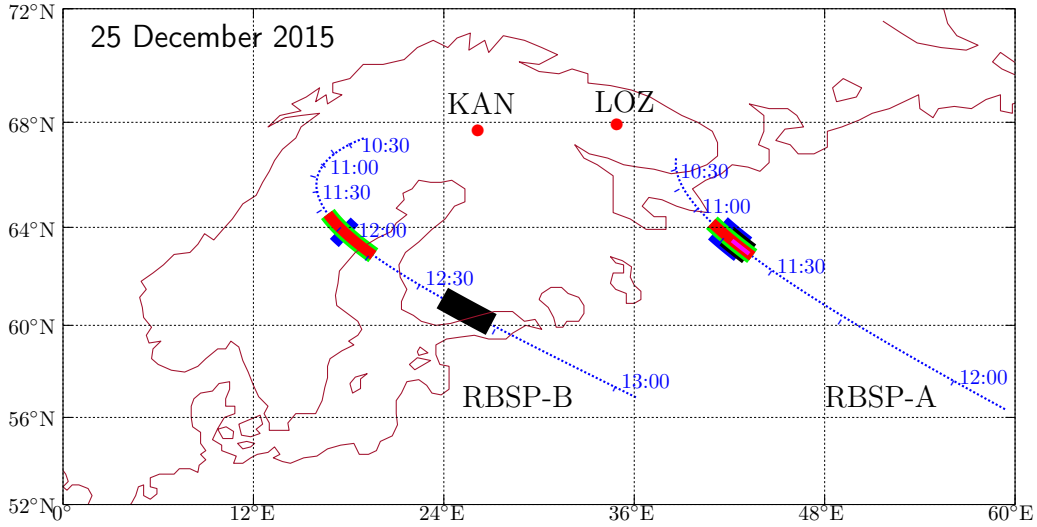


**Figure 1.** A map showing the location of KAN and LOZ ground stations (points) and the footprints of Van Allen Probes (thin lines) for the event on 25 December 2015. Thick blue segments mark the orbit parts where one-to-one correspondence of VLF emissions at the spacecraft and on the ground was observed. Green, red, and magenta segments indicate the time intervals corresponding, respectively, to low wave-normal angles (Figures 2d and 3d), Poynting vector direction from the equator (Figures 2e and 3e), and matching between the calculated growth rate and observed wave bands (Figure 6b). Black segments indicate crossing of the localized density enhancement (Figures 2e and 3e).

179 5.4 to  $L = 2.9$  in the daytime sector from 13.1 to 15.6 MLT (magnetic local time) at  
 180 the geomagnetic latitude (MLAT) from  $-5^\circ$  to  $-15^\circ$  (negative MLAT corresponds to  
 181 the southern hemisphere). RBSP-A moved from  $L = 4.6$  to  $L = 2.9$  from 11:00 to 12:00 UT,  
 182 being in the afternoon sector (14.4 to 16.1 MLT) at MLAT from  $-11.6^\circ$  to  $-16.4^\circ$ .

### 183 3.1 VLF emissions observed by KAN and LOZ

184 Overview spectrograms of VLF signals detected by KAN are shown in Figures 2a  
 185 (magnetic field spectral power) and 2b (angle of the minor axis of the polarization el-  
 186 lipse, i.e., angle of arrival relative to the geographic North). In Figure 3a, the spectro-  
 187 gram is repeated for comparison with RBSP-A. The emissions were observed in two fre-

188 quency bands  $f = 3\text{--}6$  kHz and  $f = 8.5\text{--}10$  kHz. In this paper, we discuss only the  
 189 lower band, since QP emissions were observed there. In the higher frequency band  $f =$   
 190  $8.5\text{--}10$  kHz, individual bursts of narrow-band noise ( $\Delta f < 1$  kHz) were detected with  
 191 an increasing carrier frequency and duration of about 2 min; they were discussed by Titova  
 192 et al. (2017).

193 Power spectra at LOZ are similar to KAN, so we show only the inverse angle of Poynt-  
 194 ing vector direction  $\alpha_S$  (Figure 3b), since it allows us to resolve  $180^\circ$  ambiguity in the  
 195 direction finding due to the additional measurement of vertical electric field.

196 QP emissions started at KAN and LOZ before the considered interval (about 10:20 UT)  
 197 and continued with varying intensity and even breaks till 12:30 UT. The quasi-period  
 198 varied within  $\sim (20\text{--}30)$  s. In some parts of the event they were accompanied with noise  
 199 (see, e.g., the interval 11:10 to 11:30 UT). We restrict the plotting interval for better vis-  
 200 ibility. No ground-spacecraft correlation was observed before 11:00 UT. Expanded views  
 201 of quasi-periodic elements are given in Figures 4a and 5a. These spectra correspond to  
 202 the intervals of correlation with RBSP-A and RBSP-B, respectively. The broadband sig-  
 203 nal detected by KAN at about 12:01:30 UT (Figure 5a) is the interference due to a car  
 204 that was passing near the antennas.

205 It is seen in Figure 5a that the QP elements detected on the ground have a fine struc-  
 206 ture and consist of discrete elements with increasing frequency and the repetition rate  
 207 of 4 s. This modulation corresponds to periodic emissions within QP emissions reported  
 208 by Engebretson et al. (2004) and Manninen et al. (2014). Similar structure was observed  
 209 during the interval shown in Figure 4a but it is less clearly visible. Sometimes there were  
 210 chorus elements in the upper part of the QP emissions at frequencies around 5 to 7 kHz  
 211 that were also observed by RBSP (Demekhov et al., 2017).

212 The angle between the minor axis of polarization ellipse and the direction to ge-  
 213 ographic North or South is shown in Figure 2b. It remains within the range of  $50^\circ\text{--}70^\circ$   
 214 during the entire event and indicates that the waves arrived at KAN either from north-  
 215 west or south-east. Taking into account that whistler-mode waves are generated below  
 216 the equatorial electron gyrofrequency, and  $f_{c\text{eq}} \approx 5.3$  kHz at the  $L$  shell of KAN, the  
 217 latter case seems more physically justified. This is consistent with the LOZ data presented  
 218 in Figure 3b.

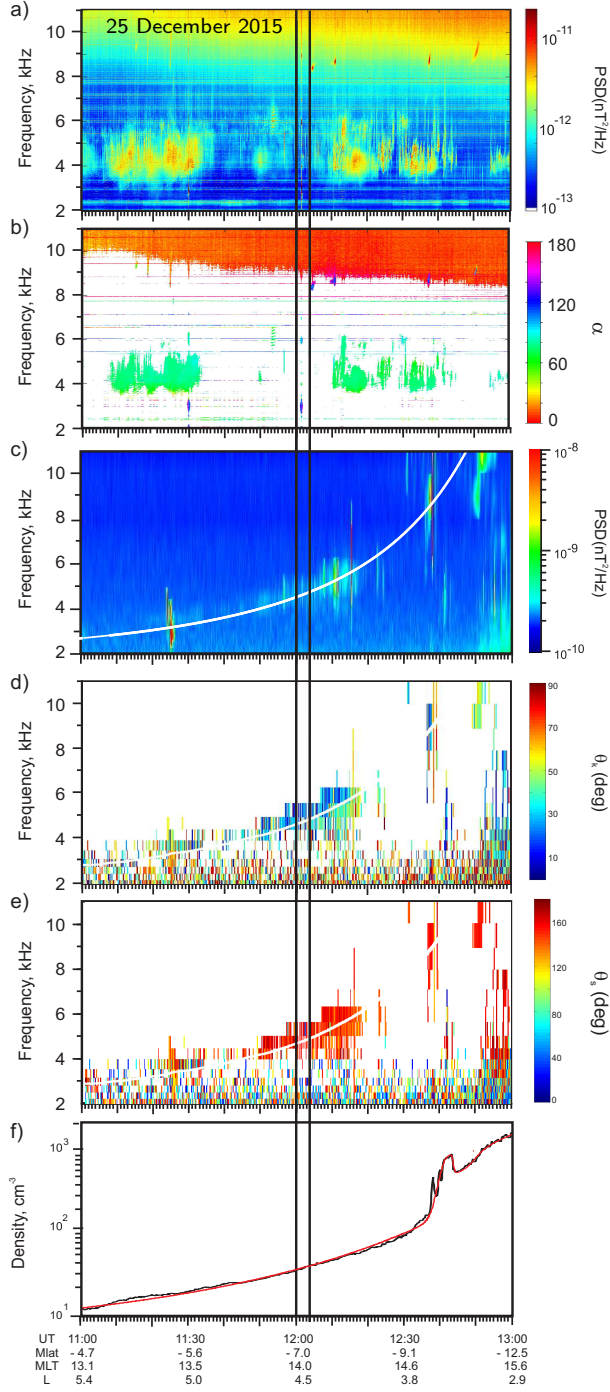


**Figure 2.** Frequency-time spectrograms of VLF emissions measured at KAN (a and b) and by the RBSP-B (c to e) on 25 December 2015 from 11:00 UT to 13:00 UT. (a) and (c) Magnetic power spectral density; (b) angle of arrival; (d) polar wave normal angle in the field-aligned coordinate system; (e) polar angle of Poynting flux. White curves show one half of the equatorial electron gyrofrequency ( $f_{ceq}/2$ ). Time interval corresponding to simultaneous observations of similar signals by KAN and RBSP-B is bounded by vertical lines. (f) Electron density derived from EFW data (black) and its smooth fit (red) that is used for ray tracing (Section 4.2).

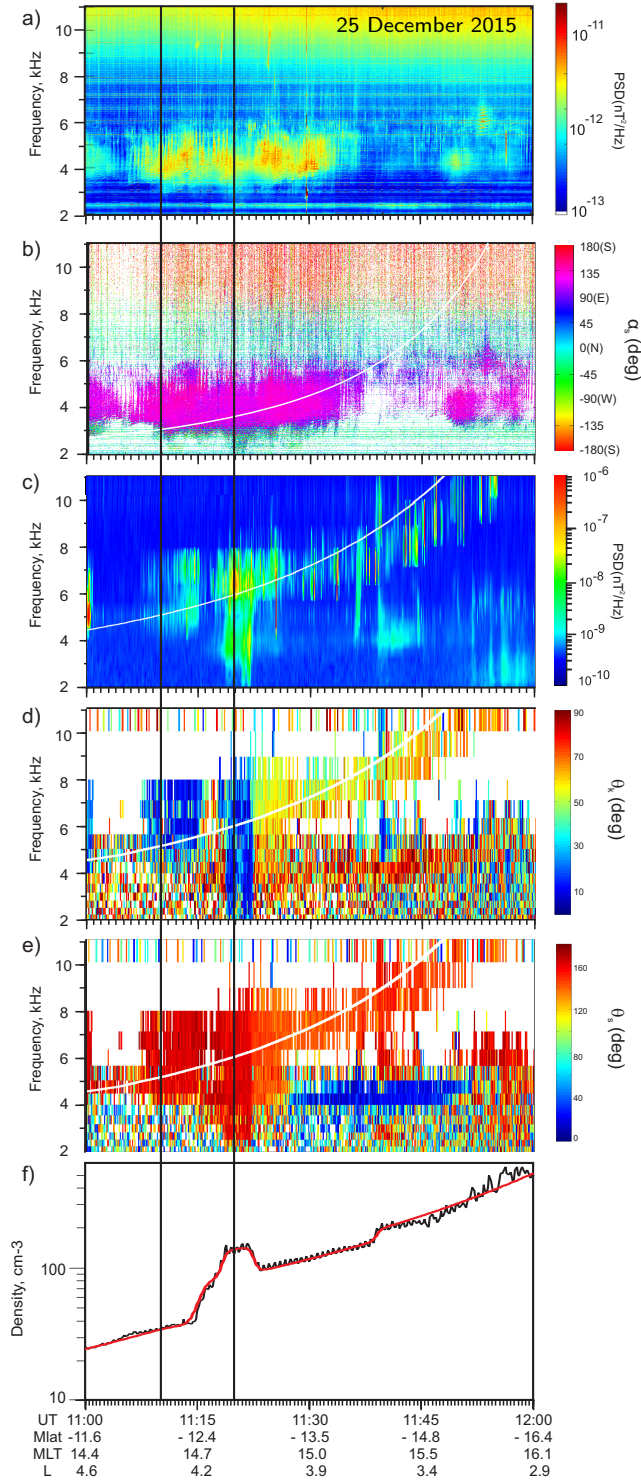


**Figure 3.** Frequency-time spectrograms of VLF emissions measured at KAN (a), LOZ (b), and by the RBSP-B (c to e) on 25 December 2015 from 11:00 to 12:00 UT. (a) and (c) Magnetic power spectral density; (b) inverse angle of Poynting flux at LOZ; (d) and (e), respectively: polar angles of wave normal and Poynting flux at RBSP-A in the field-aligned coordinate system. White curve shows one half of the equatorial electron gyrofrequency ( $f_{ceq}/2$ ) corresponding to the spacecraft  $L$ -shell. Time interval corresponding to the observations of similar signals by KAN and RBSP-A is bounded by gray vertical bars. (f) Electron density derived from EFW data (black) and its smooth fit (red) that is used for ray tracing (Section 4.2).

### 219 3.2 VLF emissions observed by RBSP

220 Overview spectrograms of VLF waves measured by RBSP-B and RBSP-A are shown  
 221 on panels c) to f) in Figures 2 and 3, respectively. We show RBSP-B first because it spent  
 222 longer time in the appropriate sector during this event. The waves are seen as multiple  
 223 amplitude enhancements, some of which are hiss and the other are chorus waves. Elec-  
 224 tron density determined by EFW measurements is plotted in Figures 2f and 3f. Some  
 225 enhancements of the wave intensity are clearly correlated with regions of enhanced plasma  
 226 density. In particular, it is true for a VLF burst observed by RBSP-A from 11:17 to 11:25 UT  
 227 in the frequency range 3–8 kHz (Figure 3c). Note that the frequency range below 2 kHz  
 228 is not shown in the plots. It contains rather intense hiss emissions which are not the fo-  
 229 cus of this paper. At KAN, there was strong interference in this frequency range, and  
 230 no natural VLF emissions were observed.

231 The overall frequency-time structure of VLF emissions detected by both RBSP space-  
 232 craft is clearly quite different compared to KAN (see Figures 2 and 3). The emission fre-  
 233 quency increased from 3–4 to 11 kHz as both spacecraft moved inward. The white and  
 234 magenta curves on the spectrograms show one half of the equatorial electron gyrofrequency  
 235  $f_{ceq}$ . The frequencies of the VLF emissions observed by RBSP remained near  $f_{ceq}/2$  dur-  
 236 ing the entire interval. All waves have almost circular right-hand polarization, i.e., be-  
 237 long to the whistler mode.

238 Figures 2d and 3c show the wave normal angles with respect to the geomagnetic  
 239 field. It is seen that VLF signals propagate in the quasiparallel mode with the wave nor-  
 240 mal angles  $\theta_k < 20^\circ$  in a time interval between 11:50 and 12:15 UT for RBSP-B and  
 241 from 11:08 to 11:23 UT for RBSP-A (in the latter case, the spacecraft observed a local-  
 242 ized density enhancement).

243 Poynting flux of the VLF waves was directed southward, i.e., away from the equa-  
 244 tor for all observed waves in the case of RBSP-B (Figure 2e) and for most of the waves  
 245 measured by RBSP-A (Figure 3e). In the case of RBSP-A one sees narrowband emis-  
 246 sions with a frequency of about 4 kHz (11:28 to 11:50 UT) and the Poynting flux directed  
 247 towards the equator which probably are reflected waves originated at higher  $L$ -shells, sim-  
 248 ilar to those reported by Parrot et al. (2003).

249 In spite of the different frequency-time structures of the VLF emissions detected  
 250 simultaneously by KAN and RBSP, these spectra turn out to be very similar during some  
 251 fairly short time intervals. These intervals are marked by vertical lines in Figures 2 and  
 252 3, and include observations of quasi-periodic emissions. They are discussed in more de-  
 253 tail below.

### 254 **3.3 Conjugate observations of QP emissions by KAN and RBSP-B**

255 Figures 4 and 5 show detailed views of conjugate KAN–RBSP observations for RBSP-  
 256 A and RBSP-B, respectively.

#### 257 ***3.3.1 Correlation with RBSP-A***

258 Figure 4 shows frequency-time spectrograms of VLF emissions obtained at KAN  
 259 (Figure 4a) and by RBSP-A (Figures 4b and 4c for magnetic and electric components  
 260 respectively) during the interval from 11:09 to 11:30 UT. At that time the spacecraft crossed  
 261 a localized plasma density enhancement of 30–40% (Figure 3f). A correspondence of the  
 262 QP elements on the ground and onboard the spacecraft can be seen in the time inter-  
 263 val 11:10 to 11:20 UT. The intensity of VLF waves observed by RBSP-A at that time  
 264 varied between  $10^{-9}$  and  $10^{-8}$  nT<sup>2</sup>/Hz. We calculated the correlation coefficient  $R$  be-  
 265 tween the spectral power of VLF waves observed at KAN and onboard RBSP-A for the  
 266 frequency channels 3983, 5019 and 5629 Hz. The interval 11:15 to 11:17 UT was excluded  
 267 from the correlation search because there was a pause in the VLF emissions measured  
 268 by RBSP-A. A better correspondence of the QP elements at RBSP-A with those at KAN  
 269 was observed for the electric field at 5019 Hz and 5629 Hz in time intervals 11:10 to 11:13 UT  
 270 and 11:17 to 11:20 UT; the correlation coefficients for these intervals are shown in Fig-  
 271 ures 4d and 4e. The maximum correlation coefficient is about 0.6, and a clear modula-  
 272 tion with the periods near 25 s and 35 s is seen in the dependence of  $R$  on the time lag  
 273 for intervals 11:10–11:13 and 11:17–11:20 UT, respectively. These periods match the QP  
 274 emission quasi-periods during the corresponding intervals.

#### 275 ***3.3.2 Correlation with RBSP-B***

276 One-to-one correspondence of the QP elements at the satellite and on the ground  
 277 is observed from 12:00 to 12:04 UT in the frequency range 3–7 kHz, when the RBSP-

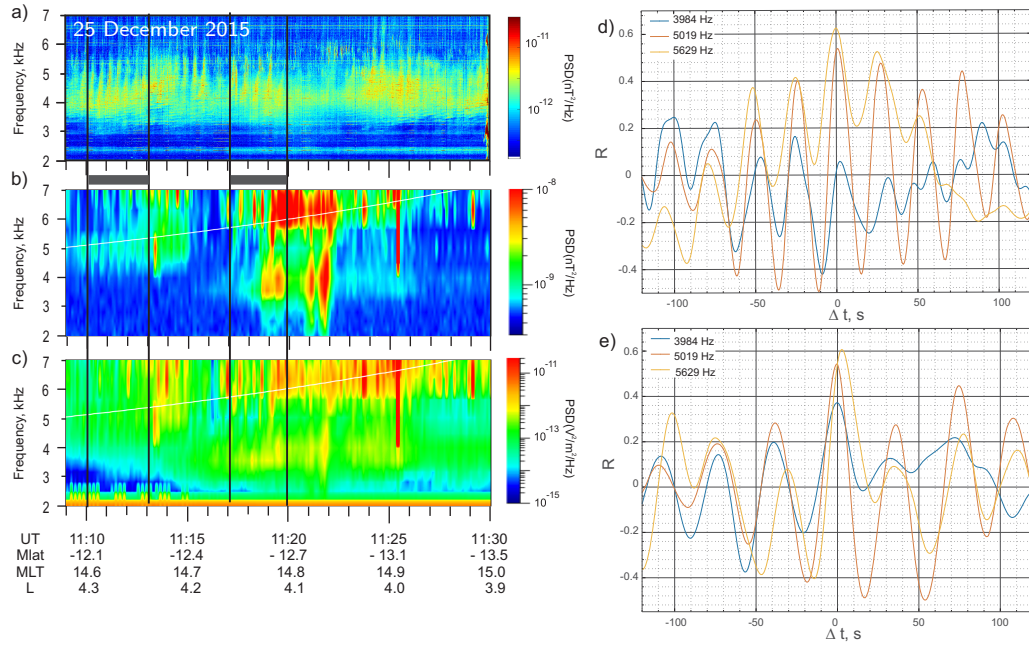


**Figure 4.** Comparison of VLF emissions observed at KAN and RBSP-A in the time interval 11:09 to 11:30 UT. (a) and (b) Magnetic power spectral density of VLF emissions detected at KAN and by RBSP-A, respectively; (c) electric power spectral density at RBSP-A; (d) and (e) correlation coefficients between the spectral powers of VLF waves measured by RBSP-A and KAN at certain frequencies in time intervals 11:10–11:13 and 11:17–11:20 UT, respectively.

278 B was at  $L \approx 4.5$ . At that time RBSP-B moved in the region with a rather smoothly  
 279 varying cold plasma density (Figure 2f). The QP elements are shown in Figures 5a and  
 280 5b. The maximum intensity of waves observed by the spacecraft is below  $10^{-9}$  nT<sup>2</sup>/Hz.  
 281 Figure 5c displays the correlation coefficient  $R$  between the magnetic field power of VLF  
 282 waves observed on the ground and onboard RBSP-B during the time interval shown in  
 283 Figures 5a and 5b in the frequency range from 4.5 to 6 kHz. The maximum correlation  
 284 coefficient is only about 0.5, in spite of a clear correspondence between all nine wave bursts  
 285 at KAN and RBSP-B. This is due to (i) a low cadence of EMFISIS survey mode which  
 286 is only 4 times shorter than the period of the observed bursts (25 s) and (ii) a fairly weak  
 287 signal measured by the spacecraft. There is clear modulation in the dependence of  $R$  on  
 288 the time lag between the two envelopes, and the modulation period coincides with the  
 289 period of QP emissions, which confirms correlation between these signals.

290 Unfortunately, during this time interval the RBSP-B satellite detected VLF emis-  
 291 sions only in the survey mode with a time resolution of 6 s, which does not allow us to  
 292 reveal a fine structure of the QP elements in the magnetosphere and compare it with KAN  
 293 observations (Figure 5a).

## 294 4 Discussion

295 In order to verify whether the spacecraft were near the source region of these emis-  
 296 sions we compare the obtained wave spectra with the results of calculation of the cyclotron  
 297 instability growth rate and analyze the possibility of exit of the VLF QP emissions to  
 298 the ground in the magnetic flux tubes where the spacecraft-ground correlation was ob-  
 299 served by RBSP-A and RBSP-B.

### 300 4.1 Growth rate of whistler-mode waves

301 Local growth rates of whistler mode waves were calculated by using the electron  
 302 pitch angle distribution and plasma parameters measured by RBSP spacecraft. The growth  
 303 rate was calculated by using the formulas of (Kennel & Petschek, 1966) with a transi-  
 304 tion from the particle distribution function to differential fluxes, as proposed by Cornilleau-  
 305 Wehrlin et al. (1985). The calculations were performed for the waves propagating par-  
 306 allel to the geomagnetic field. This is consistent with the low wave normal angles of QP  
 307 emissions detected by RBSP satellites for the analyzed event (see Figures 2d and 3d).

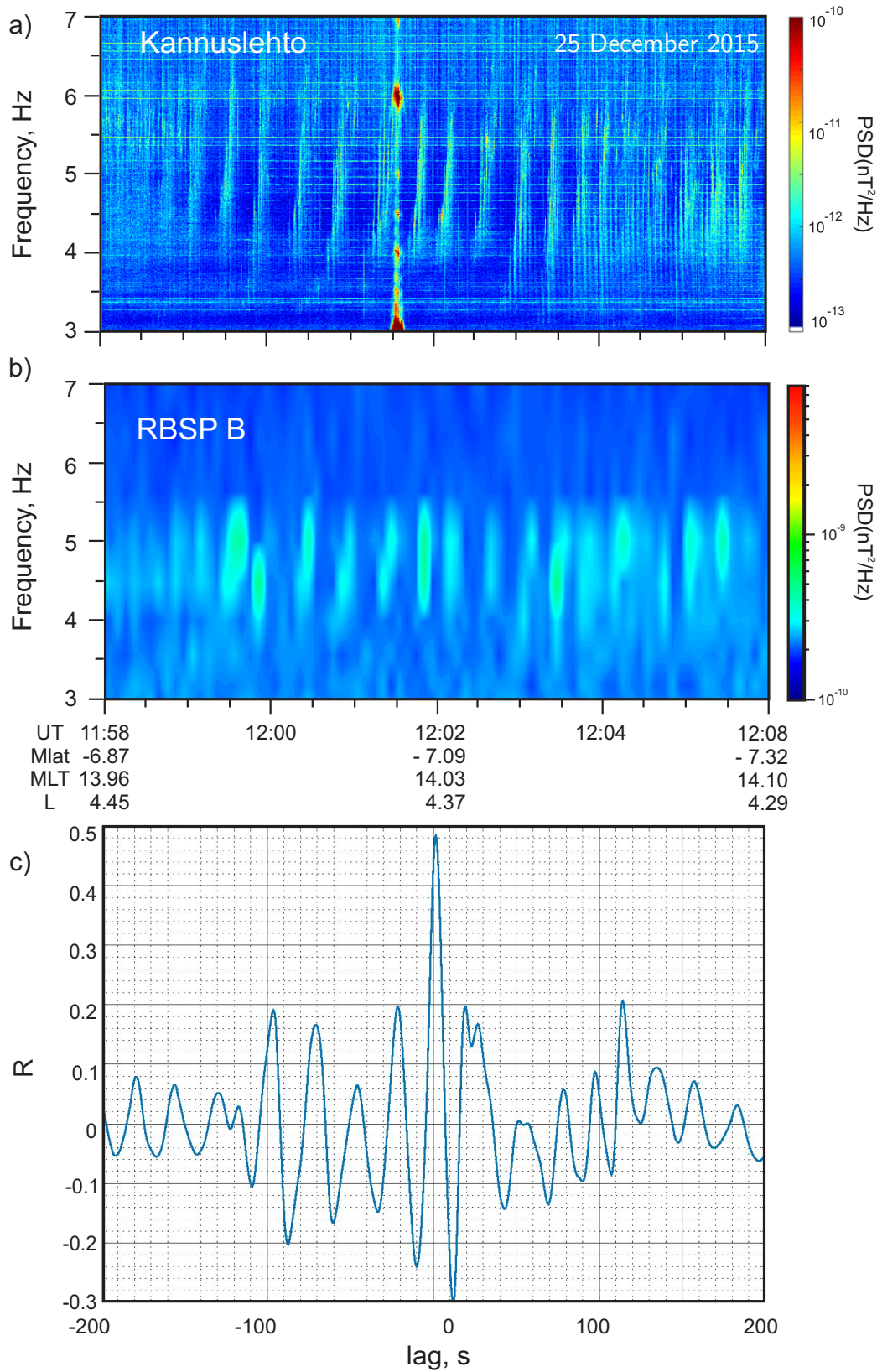


**Figure 5.** Comparison of VLF emissions observed at KAN and by RBSP-B in the time interval 12:00 to 12:04 UT. (a) and (b) Magnetic power spectral density of VLF emissions detected at KAN and by RBSP-B, respectively. (c) Correlation coefficient between the powers of VLF waves measured by RBSP-B and KAN in the frequency range 4.5 to 6 kHz.

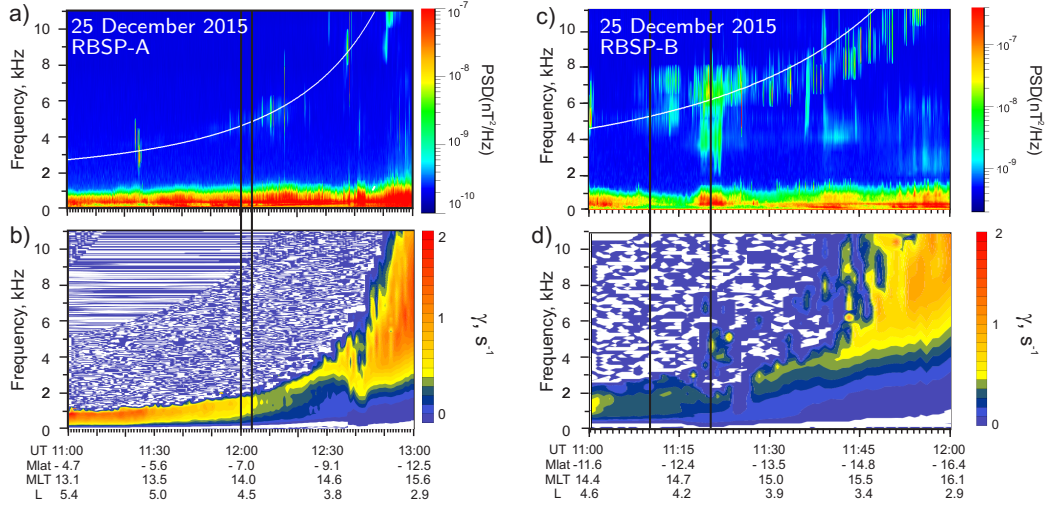


**Figure 6.** (a) and (c) Magnetic power spectral density of VLF waves; (b) and (d) growth rate of parallel propagating whistler mode waves calculated by using electron distribution functions from HOPE and MAGEIS instruments. Left and right columns show the results for RBSP-B and RBSP-A, respectively.

308 For these calculations, we averaged the HOPE and MagEIS flux data over one-minute  
 309 intervals in order to smooth the fluctuations. More details of the procedure are given in  
 310 (Lyubchich et al., 2017). Electron density profiles along the spacecraft trajectories are  
 311 shown in Figures 2f and 3f for RBSP-B and RBSP-A, respectively.

312 The results of growth rate calculations for RBSP-B are shown in Figure 6a. It is  
 313 seen that at high  $L \approx 5$  the growth rate is positive at low frequencies  $< 1$  kHz. As the  
 314 satellite moves to the lower  $L$  shells, the frequency range of positive growth rate extends  
 315 due to the rapid increasing of its upper frequency related to the increasing electron gy-  
 316 rofrequency. From a comparison of Figures 6a and 6c, it can be seen that the frequency  
 317 range of the positive growth rate is close to the range of VLF waves detected by RBSP-  
 318 B only in the beginning of the event (till 11:30 UT). At that time, the waves were ob-  
 319 served at frequencies below 1 kHz and did not reveal any quasi-periodic variation. Later,  
 320 the VLF wave spectra observed by the RBSP-B and the frequency range of the positive  
 321 growth rate differ significantly. During the observation of QP emissions correlated with  
 322 KAN at about 12 UT at frequencies of 3–6 kHz, the growth rate is negative in this fre-  
 323 quency range.

324 The results of growth rate calculations for RBSP-A data are shown in Figure 6b.  
 325 A general frequency increase in the growth rate spectrum is related to the spacecraft in-  
 326 ward motion. A localized increase in the growth rate value at frequencies 4 to 6 kHz is  
 327 evident at 11:17 to 11:25 UT. During that time, the growth rate band matched well the  
 328 band of the observed QP emissions. Note that it corresponded to the spacecraft cross-  
 329 ing of a density enhancement (Figure 3f). After 11:37 UT, the growth rate again increased  
 330 in value even more significantly, but at higher frequencies. The emissions observed by  
 331 RBSP-A at that time were not of QP type, and they were not detected at KAN.

## 332 4.2 Ray-tracing calculations

333 The waves generated in the equatorial region can be detected on the ground if they  
 334 reach the ionosphere, with a low wave normal angle with respect to the vertical direc-  
 335 tion (Helliwell, 1965; Kuzichev & Shklyar, 2010). We studied the propagation of QP emis-  
 336 sions from the equatorial region with the use of the cold-plasma density distribution mea-  
 337 sured by the RBSP satellites.

338 Properties of VLF wave propagation and, in particular, the possibility of their ob-  
 339 servation at the ground, are mainly determined by the cold-plasma density distribution,  
 340 especially, by different kinds of inhomogeneities, and by the initial wave parameters. As  
 341 we discussed above, the QP emissions observed by RBSP-A and B satellites correlated  
 342 with ground based measurements in the region with a smooth change in the cold plasma  
 343 density for RBSP-B (Figure 2f) and in vicinity of a duct with enhanced density ( $d \approx$   
 344 700 km,  $\Delta N_e/N_e \approx 45\%$ ) for RBSP-A (Figure 3f). In both cases the scale of the in-  
 345 homogeneity is much greater than the characteristic wave length in the considered fre-  
 346 quency range. This enables us to use the ray-tracing method for wave propagation mod-  
 347 eling.

348 For the ray-tracing simulations we have used smooth analytical distributions of the  
 349 plasma density  $N_e$  fitted to the measured values. These  $N_e$  profiles plotted as solid blue  
 350 and red curves in Figures 2f and 3f were used in our simulations to define the model de-  
 351 pendence of  $N_e(L)$ . The gyrotropic model was used to get the density distribution along  
 352 the geomagnetic field ( $N_e = N_{e\text{eq}}(f_c/f_{c\text{eq}})$ , where the subscript “eq” refers to the val-  
 353 ues in the equatorial plane). The geomagnetic field was considered in a dipole approx-  
 354 imation throughout the simulations.

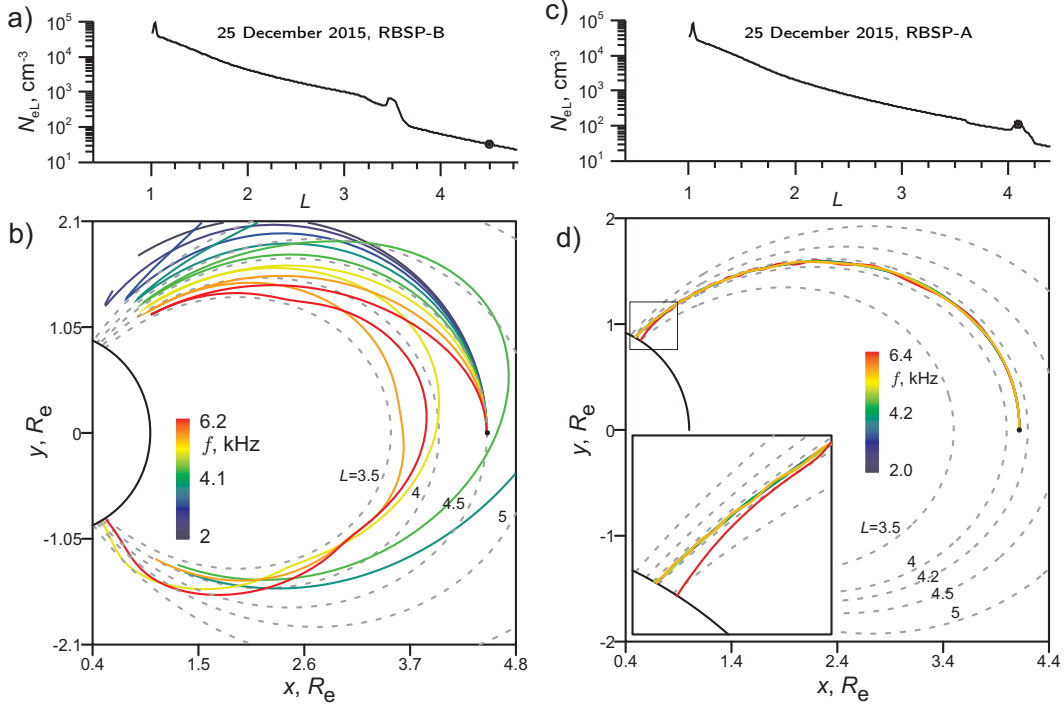


**Figure 7.** (a) and (c) Model electron density profiles used in ray tracing (see also time dependences in Figures 2f and 3f). (b) and (d) Ray trajectories of VLF waves launched with zero wave normal angle at the geomagnetic equator. The points of launch are shown by dots on the density plots. Line color encodes the frequency. Left and right columns show the results for RBSP-B and RBSP-A, respectively. Dashed gray lines show geomagnetic field lines for the  $L$  shells indicated at the lines.

355 As was mentioned above, the frequency of VLF waves observed by the spacecraft  
 356 was changing proportional to the local equatorial gyrofrequency (see Figures 2c and 3c).  
 357 This indicates that the probable source of such waves is related to the development of  
 358 the cyclotron instability (Trakhtengerts, 1963; Kennel & Petschek, 1966). This is also  
 359 supported by the measurements of the wave-normal angle which was in the range of about  
 360  $20^\circ$  at the measurement point (see Figures 2d and 3d). Thus, the starting points of rays  
 361 were chosen in the equatorial plane and the initial wave vector was directed along the  
 362 geomagnetic field ( $\theta_k = 0^\circ$ ). Due to this fact we can consider propagation of waves in  
 363 the meridional plane only.

#### 364 **4.2.1 Ray tracing from the RBSP-B location**

365 Let us consider the propagation of waves from the point at  $L = 4.5$  which cor-  
 366 responds to the RBSP-B location during simultaneous observations with KAN in the fre-  
 367 quency band 4–6 kHz (Figure 2). In this region RBSP-B observed a gradual decrease  
 368 of the plasma density with increasing distance from the Earth without noticeable irreg-  
 369 ularities (see Figure 2f). The ray tracing results for waves in frequency range 2–6 kHz  
 370 starting at the equator at  $L = 4.5$  with the wave vectors directed along the geomag-  
 371 netic field are shown in Figure 7b. It is seen that in the considered frequency range all  
 372 waves are reflected near the point at which their frequency becomes equal to the local  
 373 value of the lower-hybrid resonance (LHR) frequency (Shklyar & Jiříček, 2000), and most  
 374 of the waves do not reach the ionosphere. Only higher frequency waves with  $f \geq 5$  kHz  
 375 (which is greater than  $f_{c\text{eq}}/2 \approx 4.8$  kHz) propagate to the conjugate ionosphere after  
 376 LHR reflection, but the wave normal angles of these waves at the ionospheric level are  
 377 very high. Therefore, they were unable to pass through the ionosphere. Thus, our cal-  
 378 culations demonstrate that the waves starting from  $L = 4.5$  at the RBSP-B trajectory  
 379 could not propagate to the ground, in spite of the fact that the QP emissions observed  
 380 by RBSP-B and KAN were clearly correlated.

#### 381 **4.2.2 Ray tracing from the RBSP-A location**

382 Unlike the RBSP-B case, spectral similarity between the emissions observed by RBSP-  
 383 A and KAN in the lower frequency band (3–6 kHz) occurred in the region with the cold  
 384 plasma density duct (Figure 3e). The results of ray-tracing simulations for this case are  
 385 shown in Figure 7d. The starting point was chosen at the equator at  $L = 4.1$  (i.e., in-  
 386 side the density duct). In this case the waves at frequencies below  $f_{c\text{eq}}/2$  ( $f_{c\text{eq}} \approx 12.8$  kHz  
 387 for  $L = 4.1$ ) are trapped in the duct. However, trapping of waves with frequencies close  
 388 to the  $f_{c\text{eq}}/2$  ( $f > 6$  kHz) is violated as they approach the ionosphere (see the expanded  
 389 view of ray trajectories in the inset in Figure 7d) and afterwards the wave-normal an-  
 390 gles rapidly increases during non-ducted propagation. Thus, one should expect that only  
 391 lower frequency waves which have low wave-normal angles would propagate through the  
 392 ionosphere and could be detected by a ground station. This is consistent with KAN ob-  
 393 servations, where only waves below 6 kHz were detected (see Figures 2a and 3a).

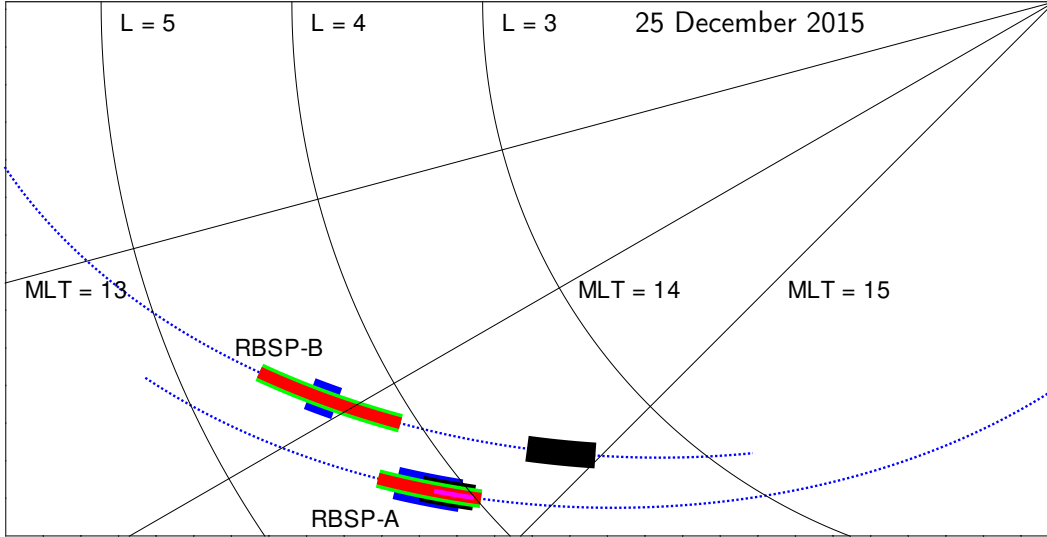


**Figure 8.** Equatorial projection of spacecraft trajectories during the event of 25 December 2015. Blue dashed lines show the trajectory parts during the time interval of QP observation at KAN. Solid blue, green, red, and magenta segments indicate the time intervals corresponding, respectively, to conjugate QP observations, low wave-normal angles, Poynting vector direction from the equator, and matching between the calculated growth rate and observed wave bands. Black segments indicate crossing of the localized density enhancement. Thin lines show fixed  $L$  and MLT values:  $L = 3, 4,$  and  $5,$  and  $MLT = 13, 14,$  and  $15$  h.

394

### 4.3 Possible location of the source of QP emissions

395

396

397

398

399

400

401

Very close similarity of QP emissions observed simultaneously by KAN and the RBSP spacecraft suggests a common source of these emissions. During both correlation intervals described above, the spacecraft observed the QP emissions at close  $L$  shells ( $L = 4.5$  for RBSP-B and  $L = 4.4$  to  $4.1$  for RBSP-A). However, these regions were separated rather far in longitude: the distance between them in geographical longitude was  $\Delta\lambda \approx 25^\circ$  (see Figure 1), and the MLT difference was about 0.7 h. The equatorial projection of spacecraft trajectories is shown in Figure 8.

402

403

404

405

The wave normal angles of the observed emissions were low in both cases of one-to-one correlation. The Poynting flux was directed away from the equator, which would be consistent with the source location in both regions. However, other data support the source location in only one of them.

406 Indeed, KAN and LOZ angles of arrival (Figures 2b and 3b) indicate the wave prop-  
 407 agation in the north-west direction. This agrees well with the wave exit to the ground  
 408 from the flux tube crossed by RBSP-A from 11:15 to 11:30 UT. On the other hand, this  
 409 direction does not match the geomagnetic projection of RBSP-B at 12:00 to 12:04 UT  
 410 that was south-west from KAN.

411 The same conclusion can be drawn from calculations of whistler mode growth rate:  
 412 the band of positive growth rate corresponded well to the observed emission band along  
 413 the RBSP-A trajectory from 11:15 to 11:25 UT, but did not correspond to the QP emis-  
 414 sions detected by RBSP-B from 12:00 to 12:04 UT.

415 Moreover, the possibility of wave propagation in the ducted regime and their exit  
 416 to the ground is confirmed for observations at RBSP-A but not RBSP-B (cf. Figures 7b  
 417 and 7d). Recall that QP emissions onboard RBSP-B were correlated with those observed  
 418 by KAN in the region with a rather smooth change in the cold plasma density, whereas  
 419 the correlation between KAN and RBSP-A was observed when the spacecraft was in the  
 420 vicinity of a region (duct) with enhanced plasma density.

421 To summarize, we think that the entire data set supports the location of possible  
 422 source region of the considered QP emissions in or very close to the flux tube crossed  
 423 by RBSP-A from 11:15 to 11:30 UT. Based on KAN and LOZ angles of arrival, which  
 424 practically did not change during the considered time interval, the source region remained  
 425 stable with respect to the ground stations during the entire observation interval from 11:10  
 426 to 12:40 UT. This stability can be explained by association of this possible source region  
 427 with a plasma density duct, that could corotate with the Earth and thus remain stable  
 428 with respect to KAN and LOZ. Indeed, the geomagnetic activity was low, with  $K_p \sim$   
 429  $2.0$  and  $Dst \sim -4$  nT, and the electric field measured by EFW onboard the RBSP-A  
 430 and RBSP-B (not shown here for brevity) was almost equal to the corotation field, which  
 431 confirms our assumption.

432 An enhancement of plasma density was also recorded by RBSP-B at 12:38 to 12:43 UT  
 433 (Figure 2f). The projection of this enhancement shown in Figure 8 matches well the MLT  
 434 sector at which the duct was detected by RBSP-A more than one hour before. There-  
 435 fore, the observed plasma structure remained fairly stable even after the end of the QP  
 436 event. The question how the waves propagated from their probable generation region  
 437 (which, as we think, was crossed by RBSP-A at around 11:15 to 11:25 UT) to the re-

438 gion of their detection by RBSP-B remains open. Note that the propagation took place  
 439 in both radial and azimuthal directions. A related and also unresolved question is why  
 440 the waves stopped being detected by RBSP-B at 12:04 UT while they continued being  
 441 observed at KAN till 12:30 UT. Both magnetospheric refraction and propagation in the  
 442 Earth-ionosphere waveguide with subsequent wave leakage to the ionosphere should be  
 443 considered, taking into account much lower wave amplitude measured by RBSP-B out-  
 444 side the probable generation region.

445 Our results directly confirm, for this specific event, the importance of wave guid-  
 446 ing for generation of QP emissions, since their source was found in a duct with enhanced  
 447 plasma density. Previous studies (e.g., Němec et al., 2018) demonstrated that statisti-  
 448 cally but indirectly by revealing that the QP events almost always had upper frequen-  
 449 cies below one half of equatorial gyrofrequency of electrons. Another indirect confirma-  
 450 tion of this fact comes from calculations of one-hop gain of whistler mode waves, that  
 451 turns out to be about 1 or less, i.e., multiple passes through the amplification region are  
 452 necessary for wave generation (Lyubchich et al., 2017).

## 453 5 Conclusions

454 We have analyzed a case where quasi-periodic VLF emissions were observed on the  
 455 ground (KAN station in Finland and LOZ station at Kola Peninsula) and by RBSP space-  
 456 craft. Specific feature of this event was that the ground station observed the emissions  
 457 during a long time interval (10:20 to 12:30 UT), while the RBSP-A and RBSP-B space-  
 458 craft observed them during different short time intervals (11:10 to 11:20 and 12:00 to 12:04 UT,  
 459 respectively). We have revealed a plausible position of the source region of these QP emis-  
 460 sions by analyzing all available data and calculating the growth rate and ray trajecto-  
 461 ries of whistler-mode waves. This probable source region was crossed by only one space-  
 462 craft (RBSP-A), and it was related to a localized density enhancement (duct) with a scale  
 463 of 700 km across the geomagnetic field. The duct could remain stable due to low geo-  
 464 magnetic activity and almost ideal co-rotation of cold plasma. The other spacecraft de-  
 465 tected the QP emissions outside the probable source region (at a distance by 0.4 in  $L$   
 466 and 0.7 h in MLT), and with much lower power. These results directly confirm the im-  
 467 portance of guided propagation for the generation of QP emissions and demonstrate trans-  
 468 verse spreading of VLF waves in radial and azimuthal directions from a localized source  
 469 flux tube.

## Acknowledgments

Comparison of spacecraft and ground-based data and modeling (A.D., L.T., D.P., A.L., and A.N.) was supported by the Russian Science Foundation (project No. 15-12-20005). The work on the ground-based data was supported by the Academy of Finland under grant No. 315716. The work of O.S. was supported by MSMT CR through the LTAUSA17070 project and by the Praemium Academiae Award from The Czech Academy of Sciences. The authors would like to thank the designers of Van Allen Probes and developers of the instruments (EMFISIS — Craig Kletzing, EFW — John Wygant, HOPE — Herb Funsten, MagEIS — Bern Blake) for the open access to the data. Processing and analysis of the [HOPE, MagEIS, REPT, or ECT] data was supported by Energetic Particle, Composition, and Thermal Plasma (RBSP-ECT) investigation funded under NASA's Prime contract no. NAS5-01072. Van Allen Probe data used in this paper can be found in the EMFISIS (<http://emfisis.physics.uiowa.edu/data/index>), EFW (<http://www.space.umn.edu/rbspefw-data/>), and RBSP-ECT (<http://www.RBSP-ect.lanl.gov/>) archives. KAN data are available at [http://www.sgo.fi/pub\\_vlf/](http://www.sgo.fi/pub_vlf/). LOZ data are available at <http://pgia.ru/opendata/>.

## References

- Blake, J. B., Carranza, P. A., Claudepierre, S. G., Clemmons, J. H., Crain, W. R., Dotan, Y., ... Zakrzewski, M. P. (2013). The Magnetic Electron Ion Spectrometer (MagEIS) Instruments Aboard the Radiation Belt Storm Probes (RBSP) Spacecraft. *Space Sci. Rev.*, *179*(1), 383–421. doi: 10.1007/s11214-013-9991-8
- Bortnik, J., Thorne, R. M., Li, W., Angelopoulos, V., Cully, C., Bonnell, J., ... Roux, A. (2009). An observation linking the origin of plasmaspheric hiss to discrete chorus emissions. *Science*, *324*(5928), 775–778. doi: 10.1126/science.1171273
- Chum, J., & Santolík, O. (2003). Propagation of whistler-mode chorus to low altitudes: divergent ray trajectories and ground accessibility. *Ann. Geophys.*, *23*(12), 3727–3738. doi: 10.5194/angeo-23-3727-2005
- Cornilleau-Wehrin, N., Solomon, J., Korth, A., & Kremser, G. (1985). Experimental study of the relationship between energetic electrons and ELF waves observed on board GEOS: A support to quasi-linear theory. *J. Geophys. Res.*, *90*(A5),

- 4141–4154. doi: 10.1029/JA090iA05p04141
- 502
- 503 Demekhov, A. G., Manninen, J., Santolík, O., & Titova, E. E. (2017). Conjugate  
 504 ground–spacecraft observations of VLF chorus elements. *Geophys. Res. Lett.*,  
 505 *44*(23), 11735–11744. doi: 10.1002/2017GL076139
- 506 Engebretson, M. J., Posch, J. L., Halford, A. J., Shelburne, G. A., Smith, A. J.,  
 507 Spasojevic, M., . . . Arnoldy, R. L. (2004). Latitudinal and seasonal varia-  
 508 tions of quasiperiodic and periodic VLF emissions in the outer magnetosphere.  
 509 *J. Geophys. Res.*, *109*(A05). doi: 10.1029/2003JA010335
- 510 Fedorenko, Y., Tereshchenko, E., Pilgaev, S., Grigoryev, V., & Blagoveshchenskaya,  
 511 N. (2014). Polarization of ELF waves generated during ”beat-wave” heating  
 512 experiment near cutoff frequency of the Earth-ionosphere waveguide. *Radio*  
 513 *Science*, *49*(12), 1254–1264. doi: 10.1002/2013RS005336
- 514 Funsten, H. O., Skoug, R. M., Guthrie, A. A., MacDonald, E. A., Baldonado, J. R.,  
 515 Harper, R. W., . . . Chen, J. (2013). Helium, Oxygen, Proton, and Electron  
 516 (HOPE) mass spectrometer for the Radiation Belt Storm Probes mission.  
 517 *Space Sci. Rev.*, *179*(1), 423–484. doi: 10.1007/s11214-013-9968-7
- 518 Helliwell, R. A. (1965). *Whistlers and related ionospheric phenomena*. Palo Alto,  
 519 Calif.: Stanford Univ. Press.
- 520 Inan, U. S., & Bell, T. F. (1977). The plasmopause as a vlf wave guide. *J. Geophys.*  
 521 *Res.*, *82*, 2819–2827.
- 522 Kennel, C. F., & Petschek, H. E. (1966). Limit on stably trapped particle fluxes.  
 523 *J. Geophys. Res.*, *71*(1), 1–28. doi: 10.1029/JZ071i001p00001
- 524 Kletzing, C. A., Kurth, W. S., Acuna, M., MacDowall, R. J., Torbert, R. B.,  
 525 Averkamp, T., . . . Tyler, J. (2013). The Electric and Magnetic Field In-  
 526 strument Suite and Integrated Science (EMFISIS) on RBSP. *Space Sci. Rev.*,  
 527 *179*(1), 127–181. doi: 10.1007/s11214-013-9993-6
- 528 Kurth, W. S., De Pascuale, S., Faden, J. B., Kletzing, C. A., Hospodarsky, G. B.,  
 529 Thaller, S., & Wygant, J. R. (2015). Electron densities inferred from plasma  
 530 wave spectra obtained by the Waves instrument on Van Allen Probes. *J. Geo-*  
 531 *phys. Res. Space Phys.*, *120*, 904–914. doi: 10.1002/2014JA020857
- 532 Kuzichev, I. V., & Shklyar, D. R. (2010). On full-wave solution for VLF waves in  
 533 the near-Earth space. *J. Atmos. Sol.-Terr. Phys.*, *72*(13), 1044–1056. doi: 10  
 534 .1016/j.jastp.2010.06.008

- 535 Li, W., Ma, Q., Thorne, R. M., Bortnik, J., Kletzing, C. A., Kurth, W. S., ...  
 536 Nishimura, Y. (2015). Statistical properties of plasmaspheric hiss derived  
 537 from Van Allen Probes data and their effects on radiation belt electron dynam-  
 538 ics. *jgra*, *120*(5), 3393-3405. doi: 10.1002/2015JA021048
- 539 Lyubchich, A. A., Demekhov, A. G., Titova, E. E., & Yahnin, A. G. (2017).  
 540 Amplitude–frequency characteristics of ion–cyclotron and whistler-mode  
 541 waves from Van Allen Probes data. *Geomagn. Aeron.*, *57*(1), 40–50. doi:  
 542 10.1134/S001679321701008X
- 543 Manninen, J. (2005). *Some aspects of ELF-VLF emissions in geophysical research*  
 544 (Doctoral dissertation, Sodankylä Geophysical Observatory Publications,  
 545 No. 98, [http://www.sgo.fi/Publications/SGO/thesis/ManninenJyrki](http://www.sgo.fi/Publications/SGO/thesis/ManninenJyrki.pdf)  
 546 [.pdf](http://www.sgo.fi/Publications/SGO/thesis/ManninenJyrki.pdf)). Retrieved from [http://www.sgo.fi/Publications/SGO/thesis/](http://www.sgo.fi/Publications/SGO/thesis/ManninenJyrki.pdf)  
 547 [ManninenJyrki.pdf](http://www.sgo.fi/Publications/SGO/thesis/ManninenJyrki.pdf)
- 548 Manninen, J., Demekhov, A. G., Titova, E. E., Kozlovsky, A. E., & Pasmanik, D. L.  
 549 (2014). Quasiperiodic VLF emissions with short-period modulation and their  
 550 relationship to whistlers: A case study. *J. Geophys. Res.*, *119*(A6), 3544-3557.  
 551 doi: 10.1002/2013JA019743
- 552 Martinez-Calderon, C., Katoh, Y., Manninen, J., Kasahara, Y., Matsuda, S., Ku-  
 553 mamoto, A., ... Miyoshi, Y. (2019). Conjugate observations of dayside and  
 554 nightside VLF chorus and QP emissions between Arase (ERG) and Kannusle-  
 555 hto, Finland. *Journal of Geophysical Research: Space Physics*, *124*. doi:  
 556 10.1029/2019JA026663
- 557 Martinez-Calderon, C., Shiokawa, K., Miyoshi, Y., Keika, K., Ozaki, M., Schofield,  
 558 I., ... Kurth, W. S. (2016). ELF/VLF wave propagation at subauroral lat-  
 559 itudes: Conjugate observation between the ground and Van Allen Probes A.  
 560 *J. Geophys. Res. Space Phys.*, *121*(A6). doi: 10.1002/2015JA022264
- 561 Němec, F., Bezděková, B., Manninen, J., Parrot, M., Santolík, O., Hayosh,  
 562 M., & Turunen, T. (2016). Conjugate observations of a remarkable  
 563 quasiperiodic event by the low-altitude DEMETER spacecraft and ground-  
 564 based instruments. *J. Geophys. Res. Space Phys.*, *121*, 8790-8803. doi:  
 565 10.1002/2016JA022968
- 566 Němec, F., Hospodarsky, G. B., Bezděková, B., Demekhov, A. G., Pasmanik, D. L.,  
 567 Santolík, O., ... Hartley, D. (2018). Quasiperiodic whistler mode emissions

- 568 observed by the Van Allen Probes spacecraft. *J. Geophys. Res. Space Phys.*,  
569 *123*, 8969-8982. doi: 10.1029/2018JA026058
- 570 Němec, F., Santolík, O., Pickett, J. S., Parrot, M., & Cornilleau-Wehrin, N. (2013).  
571 Quasiperiodic emissions observed by the Cluster spacecraft and their asso-  
572 ciation with ULF magnetic pulsations. *J. Geophys. Res. Space Phys.*, *118*,  
573 4210-4220. doi: 10.1002/jgra.50406
- 574 Parrot, M., Santolík, O., Cornilleau-Wehrin, N., Maksimovic, M., & Harvey, C.  
575 (2003). Magnetospherically reflected chorus waves revealed by ray tracing with  
576 CLUSTER data. *Ann. Geophys.*, *21*, 1111-1120.
- 577 Santolík, O., Chum, J., Parrot, M., Gurnett, D. A., Pickett, J. S., & Cornilleau-  
578 Wehrin, N. (2006). Propagation of whistler mode chorus to low altitudes:  
579 Spacecraft observations of structured ELF hiss. *J. Geophys. Res.*, *111*(A10).  
580 doi: 10.1029/2005JA011462
- 581 Santolík, O., & Gurnett, D. A. (2002). Propagation of auroral hiss at high altitudes.  
582 *Geophys. Res. Lett.*, *29*(10), 1191-1194.
- 583 Santolík, O., & Gurnett, D. A. (2003). Transverse dimensions of chorus in the source  
584 region. *Geophys. Res. Lett.*, *30*(2). doi: 10.1029/2002GL016178
- 585 Santolík, O., Kletzing, C. A., Kurth, W. S., Hospodarsky, G. B., & Bounds, S. R.  
586 (2014). Fine structure of large-amplitude chorus wave packets. *Geophys. Res.*  
587 *Lett.*, *41*, 293-299. doi: 10.1002/2013GL058889
- 588 Santolík, O., Parrot, M., & Lefeuvre, F. (2003). Singular value decomposition meth-  
589 ods for wave propagation analysis. *Radio Sci.*, *38*(1), 1010. doi: 10.1029/  
590 2002JA009791
- 591 Santolík, O., Pickett, J. S., Gurnett, D. A., Menietti, J. D., Tsurutani, B. T., &  
592 Verkhoglyadova, O. (2010). Survey of Poynting flux of whistler mode chorus in  
593 the outer zone. *J. Geophys. Res.*, *115*(A7). doi: 10.1029/2009JA014925
- 594 Sazhin, S. S., & Hayakawa, M. (1994). Periodic and quasiperiodic VLF emissions.  
595 *J. Atmos. Terr. Phys.*, *56*, 735-753.
- 596 Semenova, V. I., & Trakhtengerts, V. Y. (1980). On specific features of the LF  
597 waveguide propagation. *Geomagn. Aeron.*, *20*(6), 1021-1027.
- 598 Shklyar, D., & Jiříček, F. (2000). Simulation of nonducted whistler spectrograms  
599 observed aboard the MAGION 4 and 5 satellites. *J. Atmos. Sol.-Terr. Phys.*,  
600 *62*(5), 347-370.

- 601 Titova, E. E., Demekhov, A. G., Manninen, J., Pasmanik, D. L., & Larchenko, A. V.  
602 (2017). Localization of the sources of narrow-band noise VLF emissions in  
603 the range 4–10 kHz from simultaneous ground-based and Van Allen Probes  
604 satellite observations. *Geomagn. Aeron.*, *57*(6), 706-718.
- 605 Titova, E. E., Kozelov, B. V., Demekhov, A. G., Manninen, J., Santolik, O., Kletz-  
606 ing, C. A., & Reeves, G. (2015). Identification of the source of quasiperiodic  
607 VLF emissions using ground-based and Van Allen Probes satellite observa-  
608 tions. *Geophys. Res. Lett.*, *42*(15), 6137-6145. doi: 10.1002/2015GL064911
- 609 Trakhtengerts, V. Y. (1963). The mechanism of generation of very low frequency  
610 electromagnetic radiation in the Earth's outer radiation belt. *Geomagn.*  
611 *Aeron.*, *3*(3), 365.
- 612 Wygant, J. R., Bonnell, J. W., Goetz, K., Ergun, R. E., Mozer, F. S., Bale, S. D.,  
613 ... Tao, J. B. (2013). The electric field and waves instruments on the Radia-  
614 tion Belt Storm Probes (RBSP) mission. *Space Sci. Rev.*, *179*(1), 183-220. doi:  
615 10.1007/s11214-013-0013-7